Journal of Inorganic and Organometallic Polymers and Materials (2023) 33:1005–1015
https://doi.org/10.1007/s10904-023-02554-7

RESEARCH

Facile Synthesis and Characterization of Sodium Magnesium Silicate Hydrate/Sodium Magnesium Silicate Hydroxide as Novel Nanostructures for the Efficient Removal of Methylene Blue Dye from Aqueous Media

Asma S. Al-Wasidi[1] · Maram T. Basha[2] · Reem M. Alghanmi[2] · Eida S. Al-Farraj[3] · Ehab A. Abdelrahman[3,4]

Received: 6 January 2023 / Accepted: 22 January 2023 / Published online: 2 February 2023

Abstract
Methylene blue dye can cause damage to the eyes of humans and animals, as well as skin irritation. Also, it can result in nausea, cancer, vomiting, convulsions, and diarrhea. Consequently, in this work, an aqueous solution of sodium metasilicate pentahydrate (12 g dissolved in 50 mL of deionized water) reacted separately with two aqueous solutions of magnesium nitrate hexahydrate (8.47 g dissolved in 50 mL of deionized water and 11.47 g dissolved in 50 mL of deionized water) to obtain sodium magnesium silicate hydrate/sodium magnesium silicate hydroxide as novel nanostructures via the sol–gel method. Besides, the synthesized nanostructures were utilized for the efficient removal of methylene blue dye from aqueous media. The mean crystallite sizes of the nanostructures, which were synthesized using 8.47 and 11.47 g of magnesium nitrate hexahydrate, are 73.17 and 60.25 nm, respectively. The nanostructures, which were synthesized using 8.47 and 11.47 g of magnesium nitrate hexahydrate, were composed of cubes, spheres, and irregular shapes with mean grain sizes of 175 and 110 nm, respectively. The BET surface areas of the nanostructures, which were synthesized using 8.47 and 11.47 g of magnesium nitrate hexahydrate, are 171.04 and 189.90 m^2/g, respectively. The maximum adsorption capacities of the nanostructures, which were synthesized using 8.47 and 11.47 g of magnesium nitrate hexahydrate, toward methylene blue dye are 384.62 and 404.86 mg/g, respectively. The adsorption of methylene blue dye using the synthesized nanostructures is consistent with the pseudo-second-order kinetic model and the Langmuir equilibrium isotherm. Also, the adsorption of the methylene blue dye is chemical and exothermic.

Keywords Sodium magnesium silicate hydrate · Sodium magnesium silicate hydroxide · Nanostructures · Adsorption · Methylene blue dye

1 Introduction

Water contamination is one of the most major environmental issues, growing at an unprecedented rate alongside industrialization. Numerous industries directly discharge varying amounts of dye wastewater into the surrounding environment, causing environmental anxiety [1–3]. The majority of dyes are consumed by textile, clothing, food, and pharmaceutical factories [4]. Because of their complicated aromatic structures, it is hard to treat synthetic dyes biologically with conventional techniques [5]. The majority of dyes are toxic, carcinogenic, infrequently biodegradable, and highly water-soluble. Dye-polluted water impacts aquatic organisms, human health, and the aesthetic appeal of water. Consequently, the treatment of wastewater is one of the main

✉ Ehab A. Abdelrahman
EAAAhmed@imamu.edu.sa; dr.ehabsaleh@yahoo.com

1 Department of Chemistry, College of Science, Princess Nourah Bint Abdulrahman University, P.O. Box 84428, Riyadh 11671, Saudi Arabia

2 Department of Chemistry, College of Science, University of Jeddah, Jeddah 21589, Saudi Arabia

3 Department of Chemistry, College of Science, Imam Mohammad Ibn Saud Islamic University (IMSIU), Riyadh 11623, Saudi Arabia

4 Chemistry Department, Faculty of Science, Benha University, Benha 13518, Egypt

challenges in environmental protection from pollutants, as it facilitates safe recycling within the ecosystem. Diverse techniques, including adsorption, coagulation sedimentation, flotation, oxidative degradation, electrochemical treatment, membrane filtration, biological, and photocatalysis, have been utilized to remove dye contaminants from wastewater [6–13]. Comparing these techniques, adsorption is regarded as a simple and effective method due to its ease of operation, low cost, high efficiency, remarkably low sludge output, and speed [14, 15]. Methylene blue (MB) dye is extensively utilized in numerous industries, including wood, linen, and silk. It is a cationic dye with high resistance to heat and light. Its release into the environment could be detrimental to human health and the environment [16]. It can cause injury to the eyes of humans and animals, as well as skin irritation. Also, it can result in nausea, cancer, vomiting, convulsions, and diarrhea as reported by Radon et al. [17]. Consequently, methylene blue dye must be eliminated from the water. Diverse adsorbents have been utilized to purify wastewater from methylene blue dye such as Fe_3O_4/kaolinite composite, kaolin/graphene oxide composite, magnetic multi-wall carbon nanotube composite, zeolite, SDBS-modified zeolite, activated carbon, and attapulgite/bentonite composite [17–23]. Isik et al. [24] synthesize boron carbon nitride using melamine and boric acid as precursors for the removal of MB dye from aqueous media. Using the Langmuir model, it was also found that the uptake capacity at 25 °C is 212.8 mg/g. Temiz et al. [25] utilized the Capsella bursa-pastoris-filled chitosan biocomposite microbeads for the removal of MB dye from aqueous media. The uptake capacity of the composite increased as the amount of Capsella bursa-pastoris increased, and the maximum uptake capacity at 25 °C was determined to be 222.22 mg/g. Li et al. [26] synthesize porous activated Starbons derived from starch for the removal of MB dye from aqueous media. The uptake capacity of the activated Starbons increase as the pH of the MB dye increases, and the maximum uptake capacity at 25 °C was determined to be 891 mg/g. Xue et al. [27] synthesize activated carbons and MOF-based composite from the ashitaba biomass for the removal of MB dye from aqueous media. The activated carbon modified by a surfactant outperformed other synthesized adsorbents made from ashitaba biomass, exhibiting uptake capacities greater than 400 mg/g. Therefore, in search of effective, economical, and new adsorbents, we have synthesized sodium magnesium silicate hydrate/sodium magnesium silicate hydroxide nanostructures as novel adsorbents for the removal of MB dye from aqueous media. The synthesized adsorbents are more effective than activated carbon in removing MB dye for several reasons, namely: 1: The adsorbents were synthesized using simple and low-cost chemicals such as magnesium nitrate and sodium metasilicate. 2: The adsorbents were synthesized in a short time using an inexpensive and environmentally friendly sol–gel method because they do not use ignition furnaces or other devices that consume electricity and do not produce toxic gases that pollute the environment, which is the opposite of what happens in the case of preparing activated carbon. 3: The adsorption capacity of the synthesized adsorbents towards the MB dye is much higher than that of the activated carbon. The synthesized nanostructures were characterized using several tools such as X-ray diffraction (XRD), Fourier-transform infrared spectroscopy (FT-IR), N_2 adsorption/desorption analyzer, and field emission scanning electron microscopy (FE-SEM). Effects of pH, time, temperature, and concentration were studied. The nanostructures utilized in this study had a higher % removal of MB dye than those previously reported.

2 Experimental

2.1 Chemicals

Magnesium nitrate hexahydrate ($Mg(NO_3)_2{\cdot}6H_2O$), sodium metasilicate pentahydrate ($Na_2SiO_3{\cdot}5H_2O$), hydrochloric acid (HCl), sodium hydroxide (NaOH), and methylene blue dye ($C_{16}H_{18}N_3SCl$) were of analytical grade, supplied from the Sigma Aldrich Company, and utilized without additional chemical refining.

2.2 Synthesis of Sodium Magnesium Silicate Hydroxide/Sodium Magnesium Silicate Hydrate Nanostructures

12 g of $Na_2SiO_3{\cdot}5H_2O$ was dissolved in 50 mL of deionized water to obtain Si(IV) solution. Also, two solutions of Mg(II) ions were prepared separately by dissolving 8.47 and 11.47 g of $Mg(NO_3)_2{\cdot}6H_2O$ in 50 mL of deionized water. Each solution of Mg(II) ions is added separately to the Si(IV) solution drop by drop (rate equals one drop per second) with vigorous stirring at 570 rpm for 1 h. The produced nanostructures were filtered, washed using deionized water, and dried at 60 °C for 8 h. The samples, which were synthesized using 8.47 and 11.47 g of $Mg(NO_3)_2{\cdot}6H_2O$, were encoded as M1 and M2, respectively. It is noteworthy that two concentrations of $Mg(NO_3)_2{\cdot}6H_2O$ were studied to study their effect on the properties of the formed nanostructures such as average crystal size and morphology. The previous preparation method is called the sol–gel method. Scheme 1 represents the experimental synthetic steps of the M1 and M2 nanostructures.

2.3 Instrumentation

A Bruker D8 Advance X-ray diffraction (XRD) apparatus was used to characterize the crystalline properties of

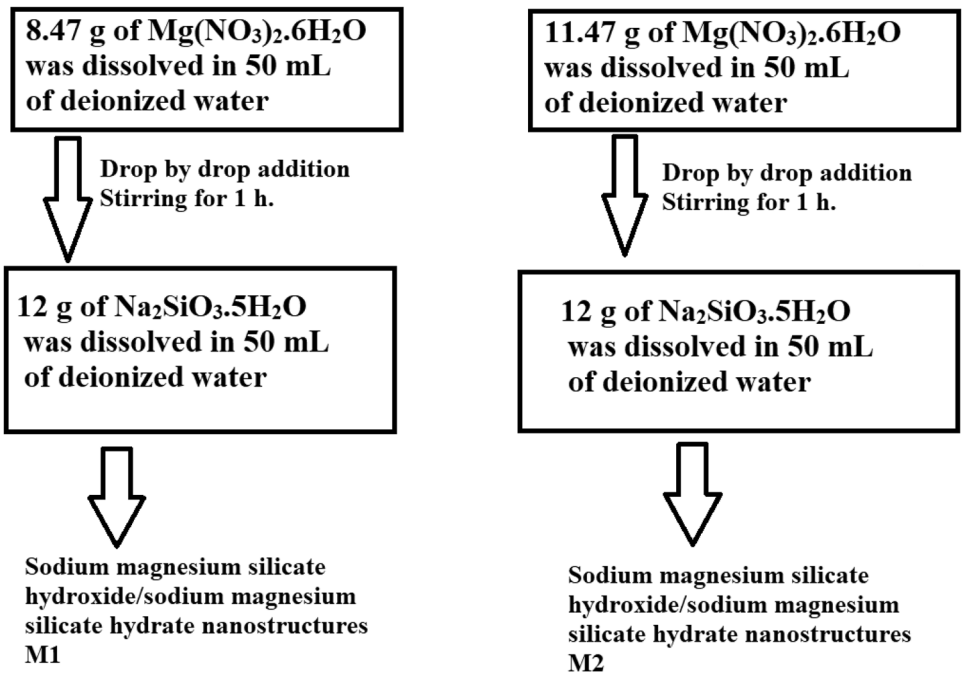

Scheme 1 The experimental synthetic steps of the M1 and M2 nanostructures

the M1 and M2 samples, where CuK_{α} wavelength equals 1.54 Å. A Nicolet iS50 Fourier transform infrared (FT-IR) instrument was utilized to identify the functional groups of the M1 and M2 samples using the KBr disc method in the wavenumber range of 4000–400 cm^{-1}. The surface morphology and elemental analysis of the M1 and M2 samples were identified using a JEOL 6510LA scanning electron microscopy (SEM) coupled to an energy-dispersive X-ray (EDX) unit. The pore characteristics and BET surface areas of the M1 and M2 samples were determined using N_2 adsorption/desorption analysis at − 196 °C on a Quantachrome NOVA Touch LX2 instrument. The concentration of the MB dye was determined using a Jasco V-670 UV–Vis spectrophotometer.

2.4 Removal of MB Dye from Aqueous Media

0.05 g of the adsorbent (M1 or M2) was completely added to 100 mL of a 200 mg/L of MB dye solution. Using 0.1 M NaOH or HCl, the pH of the mixture was adapted to the required value. The mixture was magnetically stirred at the desired time. The adsorbent was centrifuged then the MB dye concentration was measured by a Jasco V-670 UV–Vis spectrophotometer. Additionally, the maximum wavelength of the MB dye is 663 nm. Several experimental conditions were studied, for example, pH (2–8), time (10–110 min), temperature (298–328 K), and concentration (120–280 mg/L). The % removal (% R) of the MB dye and the adsorption capacity (Q) of the M1 and M2 adsorbents were calculated using Eqs. (1) and (2), respectively.

$$\%R = \frac{C_o - C_e}{C_o} \times 100 \quad (1)$$

$$Q = (C_o - C_e) \times \frac{V}{M} \quad (2)$$

where C_o represents the initial concentration of MB dye (mg/L), C_e represents the concentration of the MB dye at equilibrium (mg/L), M represents the mass of the adsorbent (g), and V represents the volume of the MB dye solution (L).

3 Results and Discussion

3.1 Characterization of the Synthesized Samples

Figure 1A and B depicts the XRD patterns of the M1 and M2 samples, respectively. Additionally, the results revealed that the M1 and M2 samples consist of two phases: sodium magnesium silicate hydrate (Chemical formula: $Na_2Mg_3Si_6O_{16}{\cdot}8H_2O$ and JCPDS No. 00-013-0310) and sodium magnesium silicate hydroxide (Chemical formula: $Na_2Mg_6Si_8O_{22}(OH)_2$ and JCPDS No. 01-030-1215). The mean crystallite sizes of the M1 and M2 samples are 73.17 and 60.25 nm, respectively. Peaks at $2\theta = 6.71°$, 19.94°, 21.19°, 27.27°, 28.22°, 30.95°, 38.92°, and 53.72° are attributable to sodium magnesium silicate hydrate. Besides, the peaks at $2\theta = 29.27°$, 35.35°, 48.19°, 55.30°, and 60.24° are due to the (060), (− 122), (500), (− 323), and (143) miller indices of sodium magnesium silicate hydroxide, respectively.

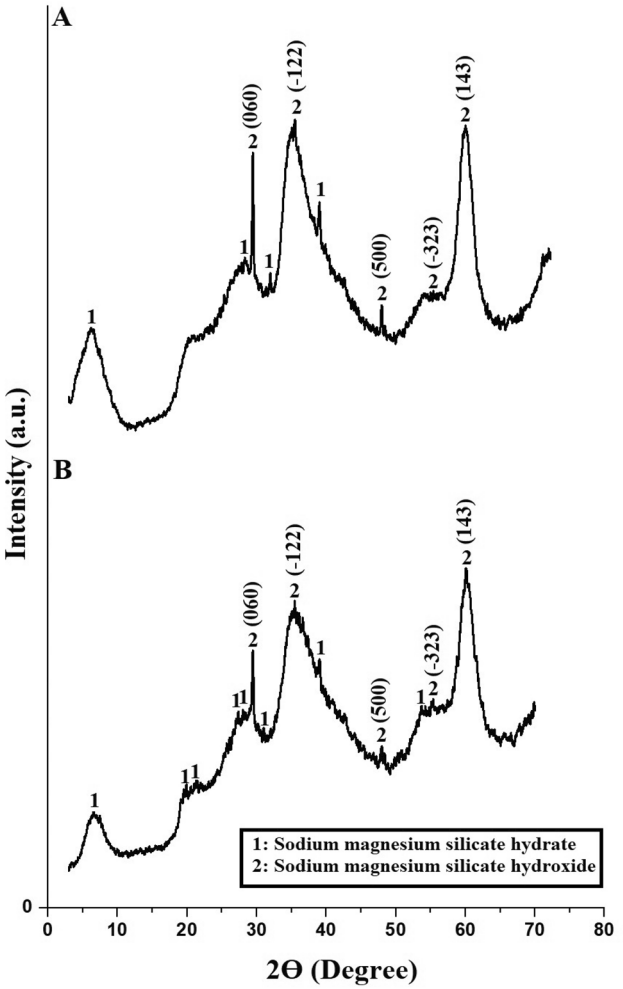

Fig. 1 The XRD patterns of the M1 (**A**) and M2 (**B**) samples

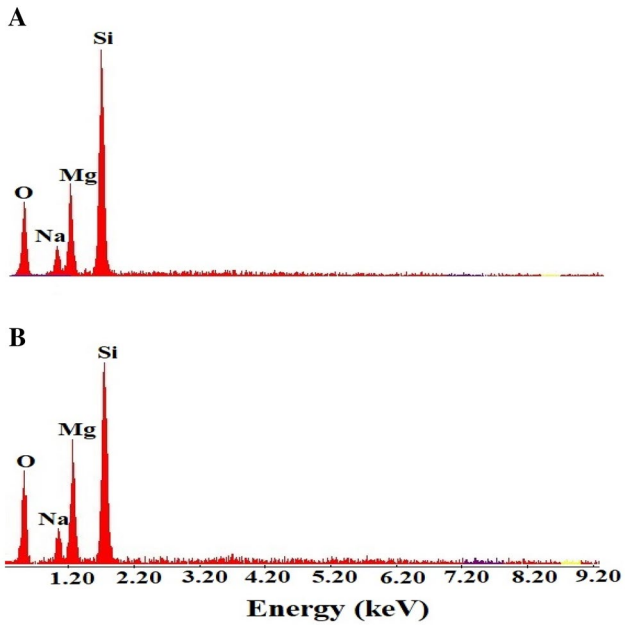

Fig. 2 The EDX patterns of the M1 (**A**) and M2 (**B**) samples

Figure 2A and B depicts the EDX patterns of the M1 and M2 samples, respectively. Additionally, the results revealed that the M1 samples is composed of Si, Mg, Na, and O with weight percentages equal to 36.82%, 17.34%, 7.53%, and 38.31%, respectively. Besides, the M2 product is composed of Si, Mg, Na, and O with weight percentages equal to 32.02%, 20.10%, 8.14%, and 39.74%, respectively.

Figure 3A and B depicts the FT-IR spectra of the M1 and M2 products, respectively. Additionally, the results confirmed that the bands, which were observed at 455 and 494 cm^{-1} in the M1 and M2 products, are due to the bending vibrations of U–O–U (U = Mg and/or Si), respectively. The observed bands at 660 and 654 cm^{-1} in the M1 and M2 products, are because of the internal symmetric stretching of U–O–U, respectively. Additionally, the bands at 902 and 910 cm^{-1} in the M1 and M2 products, are because of the external symmetric stretching of U–O–U, respectively. The bands, which were observed at 1007 and 1006 cm^{-1} in the M1 and M2 products, are because of the internal asymmetric stretching of U–O–U, respectively. Furthermore, the bands at 1390 and 1391 cm^{-1} in the M1 and M2 products, are because of the external asymmetric stretching of U–O–U, respectively. Moreover, the bands, which were observed at 1643 and 1647 cm^{-1} in the M1 and M2 products, are because of the bending vibration of O–H, respectively. The bands, which were observed at 3448 and 3466 cm^{-1} in the M1 and M2 products, are because of the stretching vibration of O–H, respectively [24, 25, 28].

Figure 4A and B depicts the FE-SEM images of the M1 and M2 products, respectively. Additionally, the results revealed that the M1 and M2 products consist of cubic, sphere, and irregular shapes with mean grain sizes of 175 and 110 nm, respectively.

Figure 5A and B depicts the N_2 adsorption/desorption isotherms of the M1 and M2 products, respectively. Additionally, the results showed that the obtained curves belong to the IV isotherm [26, 27]. An adsorption isotherm is obtained by measuring the amount of gas adsorbed across a wide range of relative pressures at a constant temperature (typically liquid N_2). Conversely, desorption isotherms are achieved by measuring the gas removed as pressure is reduced. The IV isotherm is characterized by a hysteresis loop, an initial loop (mono-multilayer adsorption), and a second loop (desorption). The IV isotherm occurs on porous adsorbents. At higher pressures, the slope shows increased uptake of adsorbate as pores become filled, and the inflection point typically occurs near the completion of the first monolayer. Also, surface properties such as BET surface area, total pore volume, and average pore size of the M1 and M2

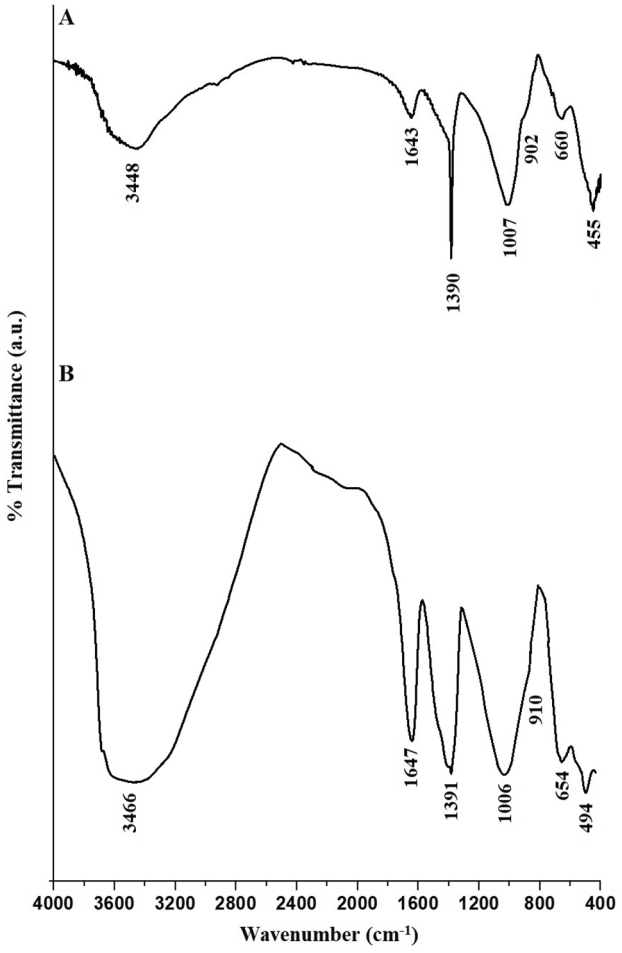

Fig. 3 The FT-IR spectra of the M1 (**A**) and M2 (**B**) samples

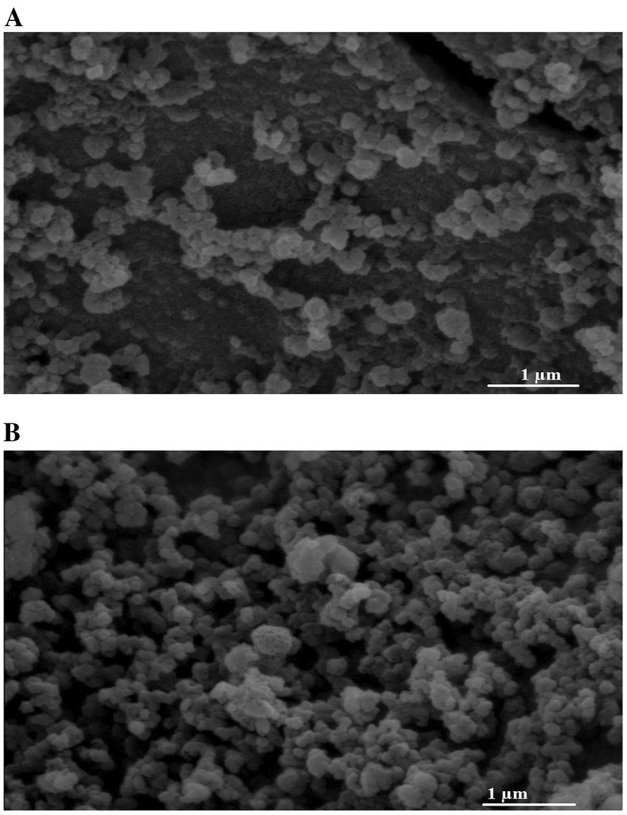

Fig. 4 The FE-SEM images of the M1 (**A**) and M2 (**B**) samples

samples are shown in Table 1. The BET surface area of the M2 sample is greater than that of the M1 sample because the mean crystallite size of the M2 sample is less than that of the M1 sample.

3.2 Removal of MB Dye from Aqueous Media

3.2.1 Effect of pH

Figure 6A and B expresses the graph of pH versus % R of MB dye and Q of the M1 and M2 samples, respectively. Increasing the pH value from 2 to 8 led to an increase in % R or Q. Therefore, at pH 8, the maximum quantity of MB dye can be eliminated. A pH higher than 8 causes the MB dye to precipitate, so the study was carried out in the range from 2 to 8 only. % R of the MB dye at pH 8 employing the M1 and M2 samples equals 93.89 and 99.30%, respectively. Also, Q of the M1 and M2 samples toward MB dye equals 375.54 and 397.18 mg/g, respectively. The point of zero charge (pH_{PZC}) is the pH of the suspension at which the net charge on the surface of an adsorbent is zero. Additionally, Fig. 7 expresses the graph of pH_{final} versus $pH_{initial}$ for several KCl solutions using the M1 and M2 samples, respectively in the same way as reported by Khalifa et al. [29]. Besides, the results showed that the pH_{PZC} of the M1 and M2 samples is 6.00 and 5.70, respectively. If the pH of the MB dye solution exceeds pH_{PZC}, both M1 and M2 are surrounded by a lot of negative ions (OH^-) on their surfaces, which can attract positive ions (MB dye) and thus increase both the % R and Q. If the pH value of the MB dye solution is smaller than pH_{PZC}, the surface of both M1 and M2 is surrounded by a lot of positive ions (H^+) that repel positive ions (MB dye) and thus decrease both the % R and Q [27, 30].

3.2.2 Effect of Time

Figure 8A and B expresses the graph of time versus % R of MB dye and Q of the M1 and M2 samples, respectively. Increasing the contact time value from 10 to 90 min led to an increase in % R or Q. Also, increasing the contact time from 90 to 110 min did not cause a significant change in % R or Q. Thus, time = 90 min is the better value at which the maximum amount of MB dye is removed. % R of the MB dye after 90 min applying the M1 and M2 samples equals 94.15

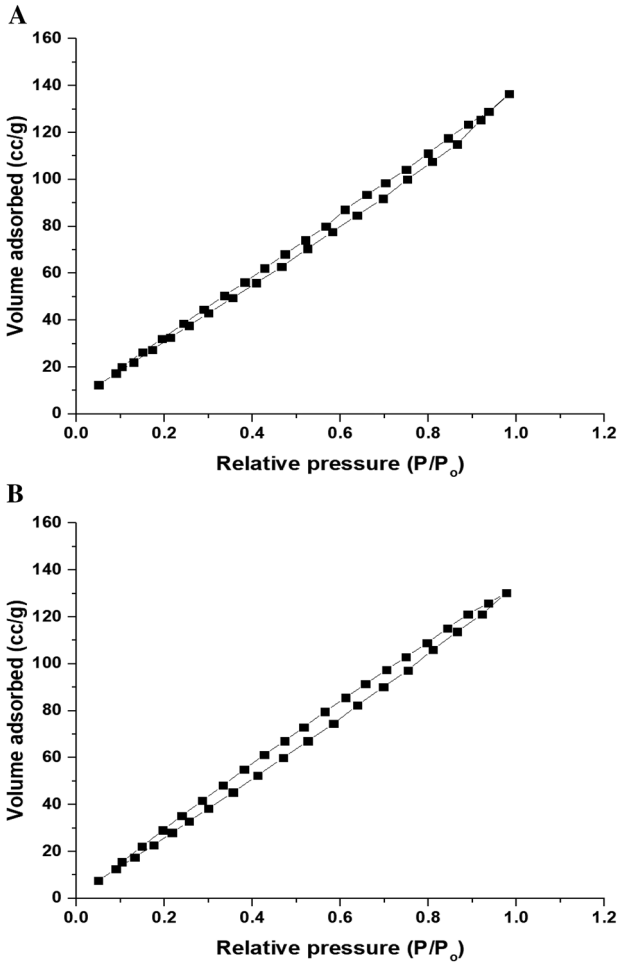

Fig. 5 The N_2 adsorption/desorption isotherms of the M1 (**A**) and M2 (**B**) samples

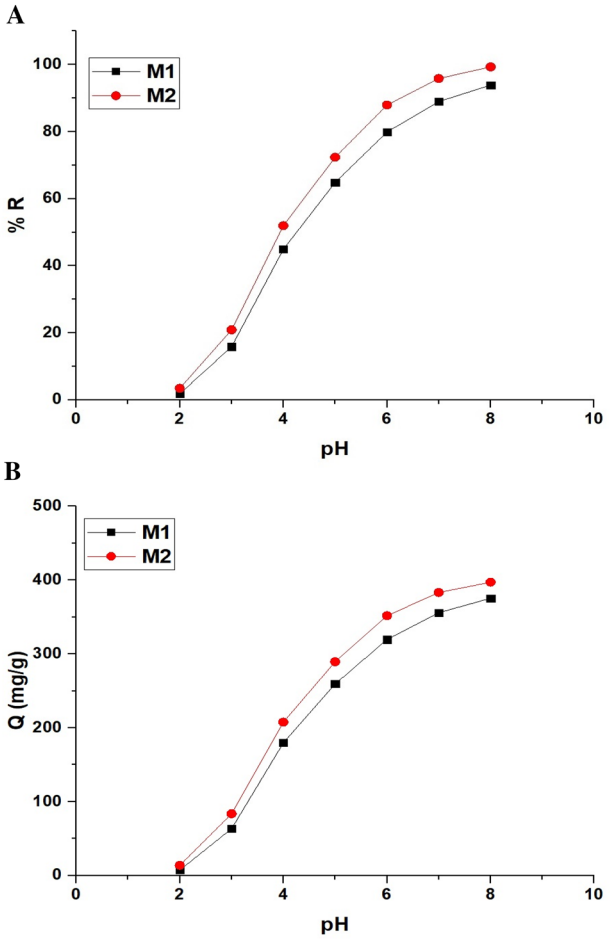

Fig. 6 The plot of pH versus % R of MB dye (**A**) and Q of the M1 and M2 samples (**B**)

Table 1 The BET surface area, average pore size, and total pore volume of the M1 and M2 products

Surface properties	Sample	
	M1	M2
BET surface area (m^2/g)	171.04	189.90
Average pore size (nm)	2.4751	2.1275
Total pore volume (cc/g)	0.2117	0.2020

and 99.25%, respectively. Also, Q of the M1 and M2 samples toward MB dye equals 376.60 and 397.00 mg/g, respectively.

The obtained results were analyzed using the pseudo-first-order and pseudo-second-order kinetic models, as defined by Eqs. (3) and (4), respectively [27, 30].

$$\log\left(Q_e - Q_t\right) = logQ_e - \frac{k_1}{2.303}t \quad (3)$$

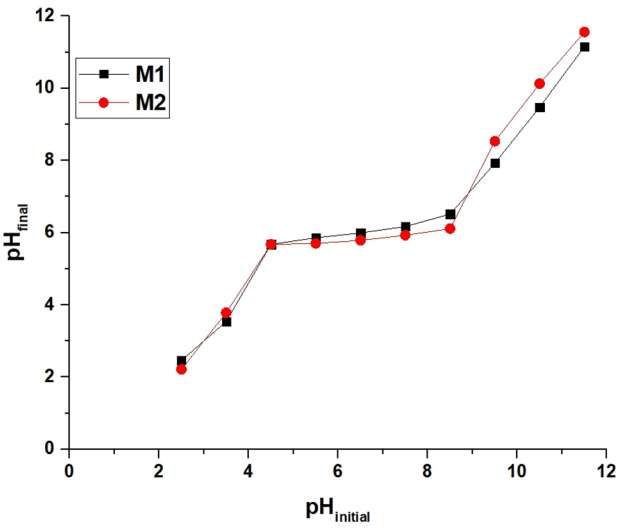

Fig. 7 The plot of pH_{final} versus $pH_{initial}$ for several KCl solutions using the M1 and M2 samples

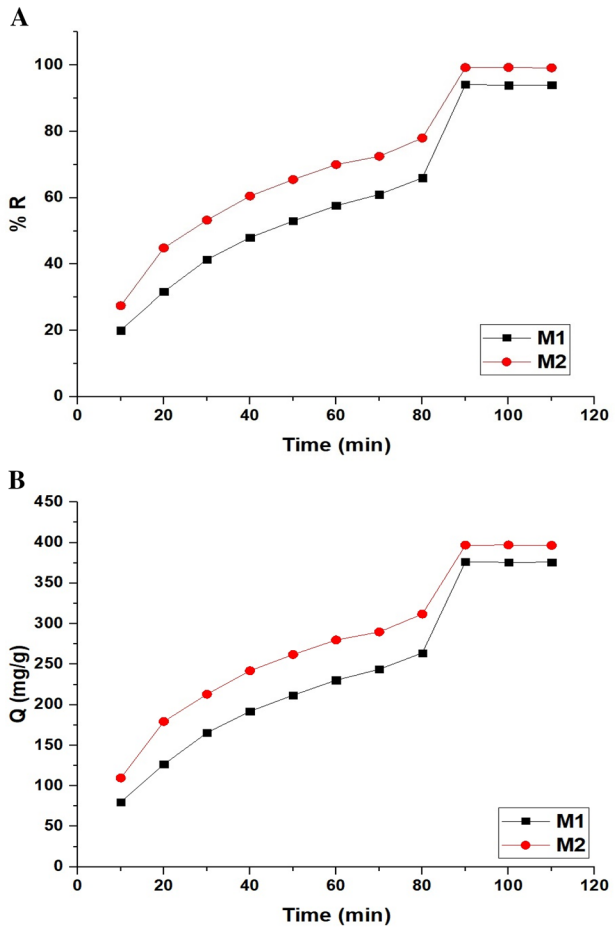

Fig. 8 The plot of time versus % R of MB dye (**A**) and Q of the M1 and M2 samples (**B**)

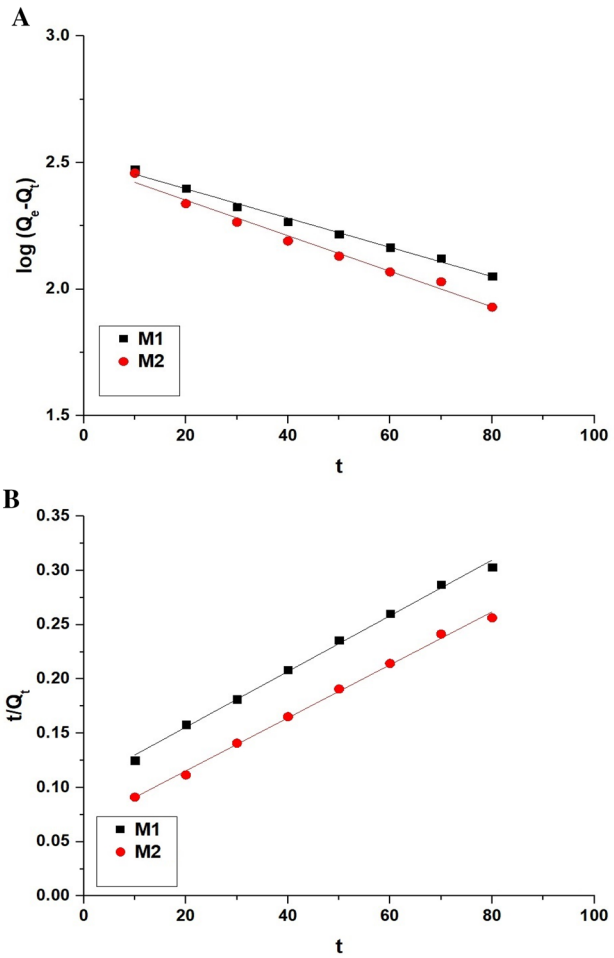

Fig. 9 The plots of log ($Q_e - Q_t$) (**A**) and t/Q_t (**B**) versus t

$$\frac{t}{Q_t} = \frac{1}{k_2 Q_e^2} + \frac{1}{Q_e} t \tag{4}$$

where Q_t (mg/g) is the quantity of MB dye adsorbed at time t (min). Q_e (mg/g) is the adsorption capacity of the M1 and M2 samples at equilibrium. k_1 is the rate constant of the pseudo-first-order model (1/min) whereas k_2 is the rate constant of the pseudo-second-order model (g/mg/min). Figure 9A and B represents the plots of log (Q_e-Q_t) and t/Q_t versus t, respectively. Also, Table 2 contains the constants of the pseudo-first-order and pseudo-second-order kinetic models. Due to the large value of the pseudo-second-order correlation coefficient (R^2) compared to its counterpart in the pseudo-first-order, the results are more consistent with the pseudo-second-order model.

3.2.3 Effect of Temperature

Figure 10A and B expresses the plot of temperature versus % R of MB dye and Q of the M1 and M2 samples, respectively. Increasing the temperature value from 298 to 328 K led to a decrease in % R or Q. Therefore, temperature = 298 K is the best value at which the maximum amount of MB dye is removed. On the basis of the experimental data, the thermodynamic parameters of adsorption processes of the MB dye applying the M1 and M2 samples, ΔG° (change in free energy, kJ/mol), ΔH° (change in enthalpy, kJ/mol) and ΔS° (change in entropy, kJ/mol kelvin), were calculated using Eqs. (5), (6), and (7) [27, 30].

$$lnK_d = \frac{\Delta S^o}{R} - \frac{\Delta H^o}{RT} \tag{5}$$

$$\Delta G^o = \Delta H^o - T\Delta S^o \tag{6}$$

$$K_d = \frac{Q_e}{C_e} \tag{7}$$

R (kJ/mol kelvin) is the gas constant. T (kelvin) is the absolute temperature whereas K_d (L/g) is the distribution constant. Figure 11 expresses the plot of ln K_d versus 1/T.

Table 2 The constants of the pseudo-first-order and pseudo-second-order kinetic models

Adsorbent	Q_e (mg/g)		Constants		R^2	
	First order	Second order	k_1 (1/min)	k_2 (g/mg/min)	First order	Second order
M1	324.98	389.11	0.0133	$6.33\times10^{5-}$	0.9916	0.9958
M2	310.29	409.84	0.0162	$8.95\times10^{5-}$	0.9823	0.9968

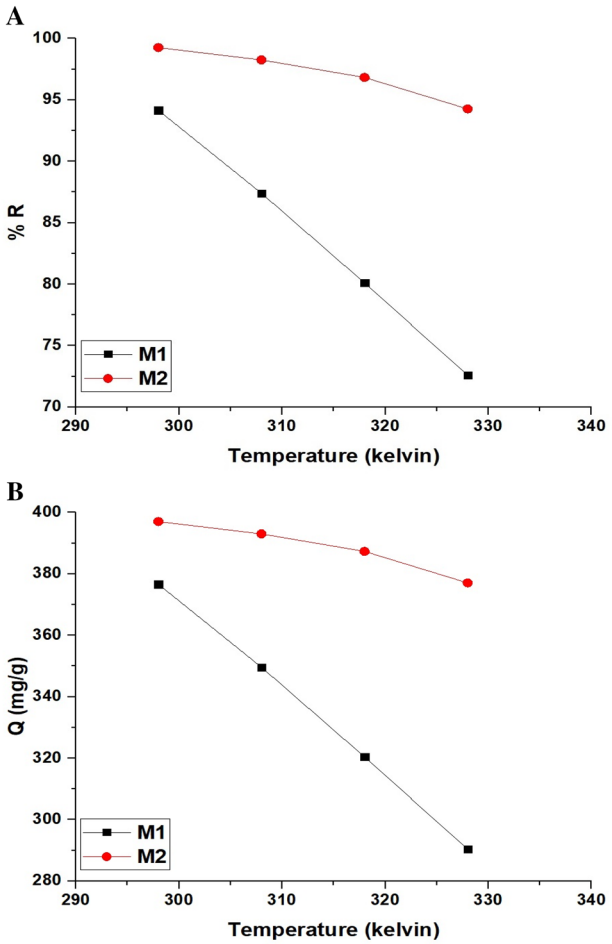

Fig. 10 The plot of temperature versus % R of MB dye (**A**) and Q of the M1 and M2 samples (**B**)

Table 3 contains the calculated thermodynamic parameters. The negative values of ΔH° and the positive values of ΔS° suggested that the adsorption processes of MB dye were conducted under exothermic nature with the increase in the system randomness. The adsorption processes of the MB dye are chemical because the ΔH° values are greater than 40 kJ/mol. The negative values of ΔG° indicated that the adsorption processes of the MB dye were spontaneous.

3.2.4 Effect of Concentration

Figure 12A and B expresses the plot of concentration versus % R of MB dye and Q of the M1 and M2 samples,

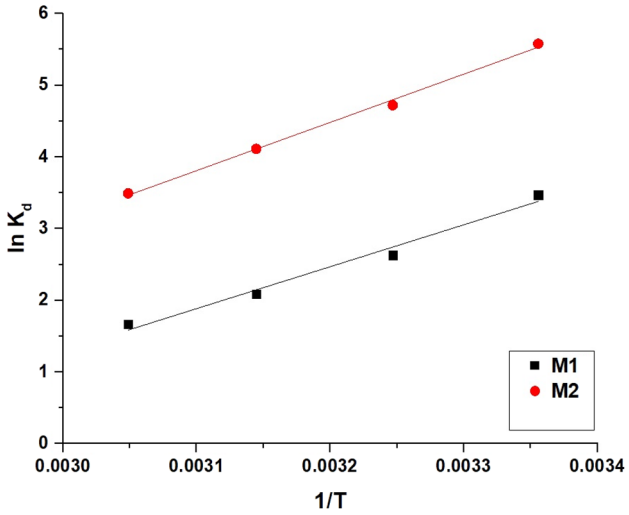

Fig. 11 The plot of $\ln K_d$ versus 1/T

respectively. Increasing the concentration value from 120 to 280 mg/L led to a decrease in % R and an increase in Q. The obtained results were analyzed using the Langmuir and Freundlich isotherms, as defined by Eqs. (8) and (9), respectively [27, 30].

$$\frac{C_e}{Q_e} = \frac{1}{k_L Q_m} + \frac{C_e}{Q_m} \tag{8}$$

$$lnQ_e = lnk_F + \frac{1}{n} lnC_e \tag{9}$$

Q_m (mg/g) represents the maximum adsorption capacity of the M1 and M2 samples. k_L (L/mg) represents the constant of the Langmuir isotherm. 1/n and k_F (mg/g)(L/mg)$^{1/n}$ are the heterogeneity constant and the constant of the Freundlich isotherm, respectively. The Freundlich isotherm can be used to determine the Q_m using Eq. (10) [27, 30].

$$Q_m = k_F\left(C_o^{1/n}\right) \tag{10}$$

Figure 13A and B expresses the Langmuir and Freundlich isotherms, respectively. Also, Table 4 contains the constants of the Freundlich and Langmuir isotherms. Due to the large value of the Langmuir correlation coefficient (R^2) compared to its counterpart in the Freundlich, the results are more consistent with the Langmuir isotherm. The maximum

Table 3 The thermodynamic constants for the removal of MB dye applying the M1 and M2 products

Adsorbent	ΔH^o (kJ/mol)	ΔS^o (kJ/mol K)	ΔG^o (kJ/mol)			
			298	308	318	328
M1	−48.86	0.1357	−89.31	−90.66	−92.02	−93.38
M2	−56.23	0.1425	−98.69	−100.11	−101.54	−102.96

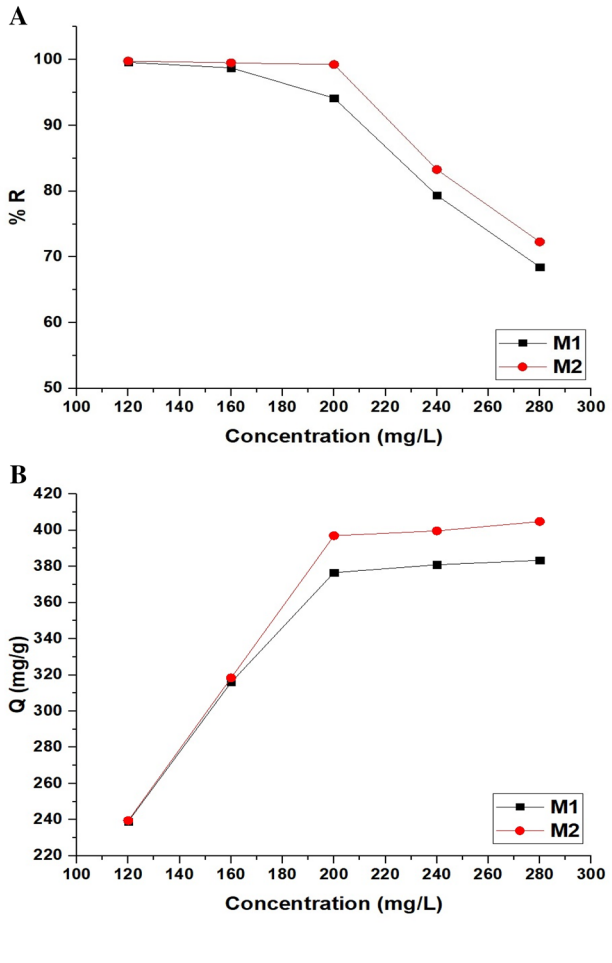

Fig. 12 The plot of concentration versus % R of methylene blue dye (**A**) and Q of the M1 and M2 samples (**B**)

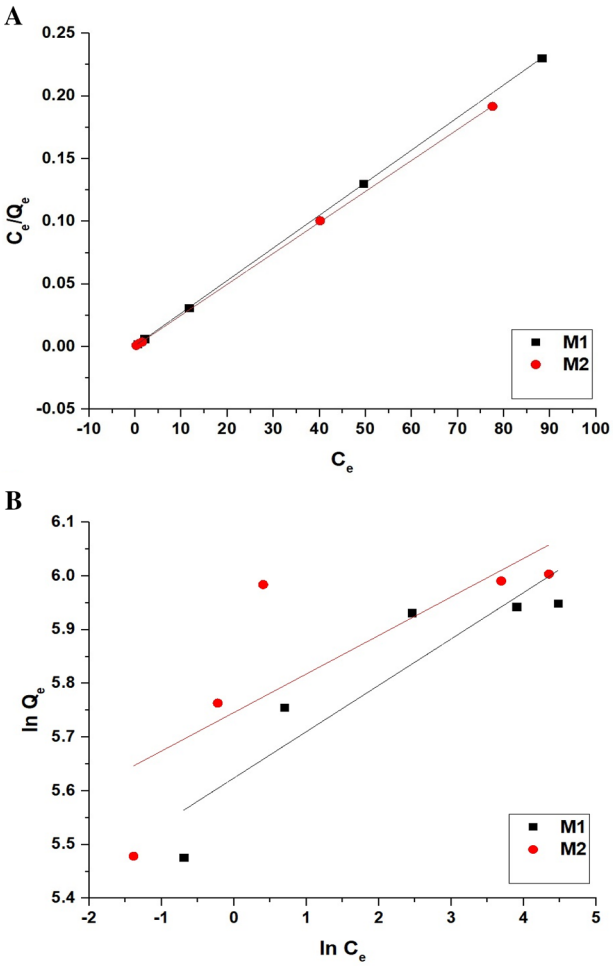

Fig. 13 The Langmuir (**A**) and Freundlich (**B**) isotherms

adsorption capacities of the M1 and M2 samples toward MB dye are 384.62 and 404.86 mg/g, respectively.

The % removal of MB dye using the M1 and M2 samples was compared with that of many adsorbents in previous studies, for example, Fe_3O_4/kaolinite composite, kaolin/graphene oxide composite, magnetic multi-wall carbon nanotube composite, zeolite, SDBS-modified zeolite, activated carbon, and attapulgite/bentonite composite, as clarified in Table 5 [17–23]. The nanostructures utilized in this study had a higher % removal of MB dye than those previously reported.

In the crystal lattice of the sodium magnesium silicate hydrate/sodium magnesium silicate hydroxide, divalent magnesium ions replace some tetravalent silicon ions,

Table 4 The calculated constants of the Langmuir and Freundlich isotherms

Adsorbent	Langmuir			Freundlich		
	Q_m (mg/g)	k_L (L/mg)	R^2	Q_m (mg/g)	k_F (mg/g)(L/mg)$^{1/n}$	R^2
M1	384.62	2.8200	0.9999	437.47	277.0007	0.7911
M2	404.86	5.1257	0.9999	457.47	312.9145	0.5073

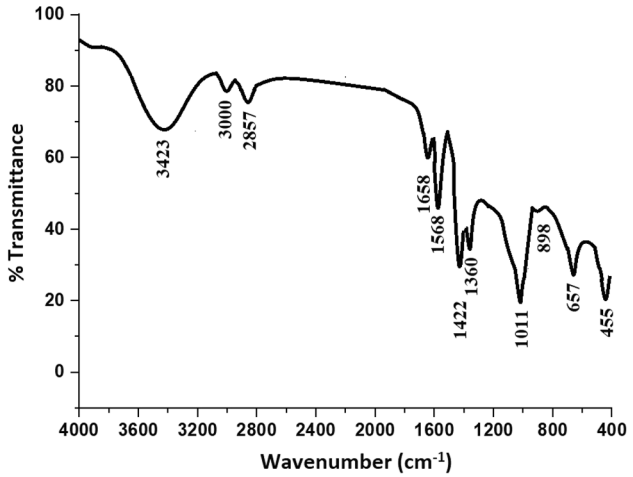

Fig. 14 The FT-IR spectrum of the MB dye adsorbed on the M1 sample

and this leads to the creation of a negative charge that is neutralized by positive sodium ions. After that, it is easy to replace positive sodium ions with other positive ions such as MB dye [16]. To confirm this adsorption mechanism, the FT-IR spectra of MB dye adsorbed on the M1 sample (as illustrative example) are shown in Fig. 14. The two bands at 3000 and 2857 cm^{-1} represent the stretching vibrations of CH aromatic and CH aliphatic of MB dye, respectively. The bands in the range 1422–1568 cm^{-1} represent the stretching vibrations of C=C aromatic of MB dye [31–35].

Table 5 Adsorption capacity of the synthesized nanostructures compared to that of further adsorbents

Adsorbent	Adsorption capacity (mg/g)	Refs.
Fe_3O_4/kaolinite composite	171.00	[18]
Kaolin/graphene oxide composite	28.016	[19]
Magnetic multi-wall carbon nanotube composite	15.87	[20]
Zeolite	8.67	[21]
SDBS-modified zeolite	15.68	[22]
Activated carbon	270.27	[23]
Attapulgite/bentonite composite	168.63	[28]
M1	384.62	This study
M2	404.86	This study

3.2.5 Regeneration and Reusability Study

To regenerate the adsorbent, MB dye is completely removed from the surface of M1 or M2 samples by heating at 180 °C for 3 h. After that, the regenerated M1 or M2 samples were used for the removal of MB dye for four consecutive cycles as previously described in the experimental part. The adsorption capacity of MB dye using the M1 and M2 samples did not change significantly as shown in Fig. 15A and B, respectively.

4 Conclusions

An aqueous solution of sodium metasilicate pentahydrate (12 g dissolved in 50 mL of deionized water) reacted with two aqueous solutions of magnesium nitrate hexahydrate (8.47 g dissolved in 50 mL of distilled water and 11.47 g dissolved in 50 mL of distilled water) to produce sodium

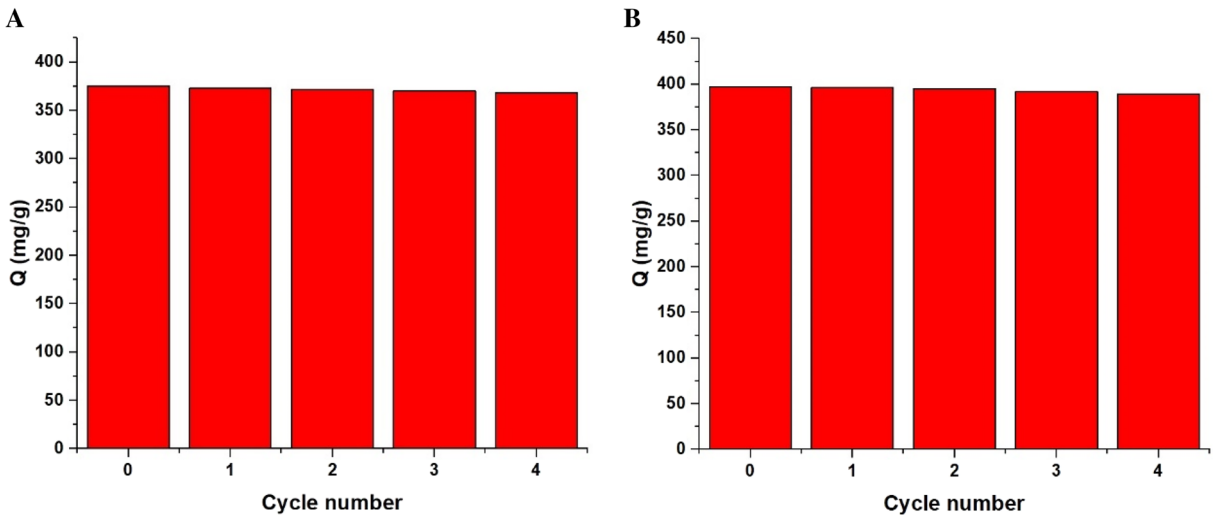

Fig. 15 The plot of the adsorption capacities of the M1 (**A**) and M2 (**B**) samples versus cycle number

magnesium silicate hydrate/sodium magnesium silicate hydroxide as novel nanostructures. M1 and M2 are the abbreviations for the nanostructures that were synthesized using 8.47 and 11.47 g of magnesium nitrate hexahydrate, respectively. The maximum adsorption capacities of the M1 and M2 samples toward MB dye are 384.62 and 404.86 mg/g, respectively.

Author contributions The authors are grateful to Princess Nourah bint Abdulrahman University, Riyadh, Saudi Arabia for funding this work through Researchers Supporting Project number (PNURSP2023R35). A.S.A. (Experimental work- Research writing - Research review), M.T.B. (Preparing figures and tables), R.M.A. (Writing the introduction-Preparing figures and tables), E.S.A. (Experimental work), E.A.A. (Idea, Experimental work, Research writing-Research review).

Funding This research was funded by Princess Nourah bint Abdulrahman University Researchers Supporting Project number (PNURSP2023R35), Princess Nourah bint Abdulrahman University, Riyadh, Saudi Arabia.

Declarations

Conflict of interest The authors confirm that there is no conflict of interest in this paper.

References

1. H. Dabhane, S. Chatur, G. Jadhav, P. Tambade, V. Medhane, Environ. Chem. Ecotoxicol. **3**, 160 (2021)
2. A. Kausar, S.T. Zohra, S. Ijaz, M. Iqbal, J. Iqbal, I. Bibi, S. Nouren, N. El Messaoudi, A. Nazir, Int. J. Biol. Macromol. **224**, 1337 (2022)
3. O. Moradi, S. Panahandeh, Environ. Res. **214**, 114042 (2022)
4. A.R. Raval, H.P. Kohli, O.K. Mahadwad, Chem. Eng. J. Adv. **12**, 100398 (2022)
5. A. Ahmad, N. Khan, B.S. Giri, P. Chowdhary, P. Chaturvedi, Bioresour. Technol. **306**, 123202 (2020)
6. H. Cao, R. Wang, K. Dou, J. Qiu, C. Peng, N. Tsidaeva, W. Wang, Environ. Res. **216**, 114730 (2022)
7. I. Chouaybi, H. Ouassif, M. Bettach, E.M. Moujahid, Inorg. Chem. Commun. **146**, 110169 (2022)
8. E.F.D. Januário, T.B. Vidovix, R. Bergamasco, A.M.S. Vieira, Chem. Eng. Process. **168**, 108577 (2021)
9. S.C.M. Signorelli, J.M. Costa, A.F. de Almeida-Neto, J. Environ. Chem. Eng. **9**, 106157 (2021)
10. L.M. Mahlaule-Glory, S. Mapetla, A. Makofane, M.M. Mathipa, N.C. Hintsho-Mbita, Heliyon **8**, e10536 (2022)
11. J. Yuan, Z. Chen, Q. Yu, W. Zhu, S. Li, L. Han, X. Lu, S. Li, Y. Wu, Z. Lv, H. You, B. Chen, J. Electroanal. Chem. **923**, 116816 (2022)
12. J. Ma, X. Tang, Y. He, Y. Fan, J. Chen, H. Yu, Desalination **480**, 114328 (2020)
13. E.A. Abdelrahman, R.M. Hegazey, S.H. Ismail, H.H. El-Feky, A.M. Khedr, M. Khairy, A.M. Ammar, Arab. J. Chem. **15**, 104372 (2022)
14. Y. Lei, J. Zhang, X. Liu, Z. Dai, X. Zhao, J. Solid State Chem. **316**, 123563 (2022)
15. Y. Zhu, Y. Cui, Y. Peng, R. Dai, H. Chen, Y. Wang, Colloids Surf. A Physicochem. Eng. Asp. **658**, 130705 (2023)
16. E.A. Abdelrahman, R.M. Hegazey, R.E. El-Azabawy, J. Mater. Res. Technol. **8**, 5301 (2019)
17. A. Radoń, S. Łoński, T. Warski, R. Babilas, T. Tański, M. Dudziak, D. Łukowiec, Appl. Surf. Sci. **487**, 1018 (2019)
18. S. Asuha, F. Fei, W. Wurendaodi, S. Zhao, H. Wu, X. Zhuang, Powder Technol. **361**, 624 (2020)
19. K. He, G. Chen, G. Zeng, A. Chen, Z. Huang, J. Shi, M. Peng, T. Huang, L. Hu, J. Taiwan Inst. Chem. Eng. **89**, 77 (2018)
20. J.L. Gong, B. Wang, G.M. Zeng, C.P. Yang, C.G. Niu, Q.Y. Niu, W.J. Zhou, Y. Liang, J. Hazard. Mater. **164**, 1517 (2009)
21. K. Rida, S. Bouraoui, S. Hadnine, Appl. Clay Sci. **83–84**, 99 (2013)
22. X. Jin, M.Q. Jiang, X.Q. Shan, Z.G. Pei, Z. Chen, J. Colloid Interface Sci. **328**, 243 (2008)
23. Y. Li, Q. Du, T. Liu, X. Peng, J. Wang, J. Sun, Y. Wang, S. Wu, Z. Wang, Y. Xia, L. Xia, Chem. Eng. Res. Des. **91**, 361 (2013)
24. B. Isik, V. Ugraskan, F. Cakar, O. Yazici, Res. Chem. Intermed. **48**, 4249 (2022)
25. R. Temiz, B. Isik, V. Ugraskan, O. Cankurtaran, Biomass Convers. Bioref. **48**, 4249 (2022)
26. H. Li, V.L. Budarin, J.H. Clark, M. North, X. Wu, J. Hazard. Mater. **436**, 129174 (2022)
27. H. Xue, X. Wang, Q. Xu, F. Dhaouadi, L. Sellaoui, M.K. Seliem, A.B. Lamine, H. Belmabrouk, A. Bajahzar, A. Bonilla-Petriciolet, Z. Li, Q. Li, Chem. Eng. J. **430**, 132801 (2022)
28. Y. Liu, Y. Kang, B. Mu, A. Wang, Chem. Eng. J. **237**, 403 (2014)
29. M.E. Khalifa, E.A. Abdelrahman, M.M. Hassanien, W.A. Ibrahim, J. Inorg. Organomet. Polym. Mater. **30**, 2182 (2020)
30. M.A. Abdelwahab, S.M. El Rayes, M.M. Kamel, E.A. Abdelrahman, Int. J. Environ. Anal. Chem. **480**, 114328 (2022)
31. E.A. Abdelrahman, R.M. Hegazey, Microchem. J. **145**, 18 (2019)
32. E.A. Abdelrahman, E.S. Al-Farraj, Nanomaterials **12**, 3992 (2022)
33. V.A. Online, H.M. Gad, S.M. El Rayes, E.A. Abdelrahman, 19209 (2022)
34. E.A. Abdelrahman, Y.G. Abou-El-Reash, H.M. Youssef, Y.H. Kotp, R.M. Hegazey, J. Hazard. Mater. **401**, 123813 (2021)
35. E.A. Abdelrahman, R.M. Hegazey, Compos. Part B Eng. **166**, 382 (2019)